A multi-temporal InSAR method incorporating both persistent scatterer and small baseline approaches

Andrew Hooper[1,2]

Received 30 May 2008; revised 10 July 2008; accepted 16 July 2008; published 19 August 2008.

[1] Synthetic aperture radar (SAR) interferometry is a technique that provides high-resolution measurements of the ground displacement associated with many geophysical processes. Advanced techniques involving the simultaneous processing of multiple SAR acquisitions in time increase the number of locations where a deformation signal can be extracted and reduce associated error. Currently there are two broad categories of algorithms for processing multiple acquisitions, *persistent scatterer* and *small baseline* methods, which are optimized for different models of scattering. However, the scattering characteristics of real terrains usually lay between these two end-member models. I present here a new method that combines both approaches, to extract the deformation signal at more points and with higher overall signal-to-noise ratio than can either approach alone. I apply the combined method to data acquired over Eyjafjallajökull volcano in Iceland, and detect time-varying ground displacements associated with two intrusion events.
Citation: Hooper, A., (2008), A multi-temporal InSAR method incorporating both persistent scatterer and small baseline approaches, *Geophys. Res. Lett.*, *35*, L16302, doi:10.1029/2008GL034654.

1. Introduction

[2] Spaceborne interferometric synthetic aperture radar (InSAR) is a valuable technique for measuring surface deformation because of the high spatial resolution achieved and the ability to acquire the data remotely. However, problems due to changes in scattering properties of the Earth's surface with time and look direction limit the applicability of InSAR. Where measurement is possible, signal due to displacement of the ground is overprinted by noise due to variation in atmospheric properties and inaccuracy in both satellite orbit and surface elevation determination.

[3] Multi-temporal InSAR (MT-InSAR) techniques, involving the processing of multiple acquisitions in time, provide one way to address these issues. Currently, there are two broad categories of MT-InSAR techniques, *persistent scatterer* (PS) methods including those that identify pixels based primarily on their phase variation in time [e.g., *Ferretti et al.*, 2001; *Kampes*, 2005] and those that use primarily correlation of their phase in space [e.g., *Hooper et al.*, 2004; *van der Kooij et al.*, 2006], and small baseline (SB) methods [e.g., *Berardino et al.*, 2002; *Schmidt and Bürgmann*, 2003]. The naming of the categories is inconsistent in that "persistent scatterer" refers to the type of pixel that is identified whereas "small baseline" refers to the methodology of interferogram formation. However, as the names are already established, I continue to use them here.

[4] In a synthetic aperture radar image, the value for each pixel is the coherent sum of contributions from all scatterers within the associated ground resolution element. Relative movement of these scatterers, or a change in the look or squint angle, causes the scatterer contributions to sum differently, an effect known as decorrelation [*Zebker and Villasenor*, 1992]. For ground resolution elements containing a persistently dominant scatterer the phase due to decorrelation varies little with time even if the dimmer scatterers move with respect to the dominant scatterer. Furthermore, the variation is also small when viewed from different look and squint angles. This is the principle behind a PS pixel. For resolution elements containing no dominant scatterer, on the other hand, phase variation due to decorrelation is often large enough to obscure the underlying signal. However, by forming interferograms only between images separated by a short time interval and with a small difference in look and squint angle, decorrelation is minimized, and for some resolution elements may be small enough that the underlying signal is still detectable. Decorrelation is further reduced by spectral filtering in range [*Gatelli et al.*, 1994] and discarding of the non-overlapping Doppler frequencies in azimuth. Pixels whose phase when thus filtered decorrelates little over short time intervals, which I refer to as slowly-decorrelating filtered phase (SDFP) pixels, are the targets of SB methods. Note that for pixels dominated by a single scatterer, the effect of range and azimuth filtering may be to increase decorrelation due to the coarsening of the resolution. Nevertheless, the decorrelation may still be low enough for many PS pixels that they also qualify as SDFP pixels. Thus SDFP pixels and PS pixels form two distinct, but potentially overlapping, sets of pixels. The phase of pixels selected by both methods will however differ due to the inclusion or absence of spectral filtering.

[5] There has been some debate about the relative merits of PS and SB approaches. However, as they are optimized for different models of ground scattering, the two approaches are in fact complementary, at least in the usual case where a data set contains pixels with a range of scattering characteristics. Here, I present a new algorithm that combines both PS and SB approaches to maximize the spatial sampling of useable signal. Improvement of the spatial sampling is important not only because the resolution of any deformation signal is increased, but also because it allows for more reliable estimation of integer phase-cycle

[1]Nordic Volcanological Center, Institute of Earth Sciences, University of Iceland, Reykjavik, Iceland.
[2]Now at Department of Earth Observation and Space Systems, Delft University of Technology, Delft, Netherlands.

0094-8276/08/2008GL034654$05.00

ambiguities present in the data (phase unwrapping). For PS selection I use the method of *Hooper et al.* [2007] and for the SB processing I use a new algorithm described in this paper. These methods are optimized for detection of deformation that is spatially correlated. After pixel selection, the two data sets are combined and further processing is performed on the combined data set to isolate the deformation signal. As a test case, I apply the algorithm to Eyjafjallajökull volcano in Iceland, which experienced intrusive episodes during 1994 and 1999–2000 [*Pedersen and Sigmundsson*, 2006].

[6] A software package to apply the PS, SB and combined MT-InSAR algorithms (StaMPS/MTI) can be downloaded from http://www.hi.is/~ahooper/stamps.

2. Methods

2.1. Persistent Scatterer Processing

[7] PS pixels are identified from interferograms optimized for PS analysis, as described by *Hooper et al.* [2007]. A minimum of five acquisitions are required. In order to process large regions on computers with an arbitrarily finite amount of memory, I have implemented an approach that splits the interferograms into a number of overlapping patches in range and azimuth. Each patch is then processed independently to identify PS pixels, which are then all combined.

2.2. Small Baseline Processing

[8] Standard SB methods [*Berardino et al.*, 2002; *Schmidt and Bürgmann*, 2003] work with interferograms that are first multi-looked and then individually phase-unwrapped. This strategy does not take advantage, however, of two of the potential benefits offered by processing multiple acquisitions together. The first is the potential to process the data at the highest possible resolution, to enable identification of isolated SDFP pixels surrounded by pixels that completely decorrelate. The second is the ability to unwrap the phase more robustly in three dimensions, the third being that of time. *Lanari et al.* [2004] have implemented a method that first identifies multi-looked SDFP pixels and then uses these to identify single-look SDFP pixels in a further step. The method I describe here differs in that it operates on single-look images to identify single-look SDFP pixels directly. Several three-dimensional phase unwrapping algorithms have recently been developed, although most are not directly applicable to InSAR time series. *Hooper and Zebker* [2007] have developed two algorithms that can be applied to single-master time series and *Pepe and Lanari* [2006] have developed a minimum cost flow algorithm that is applicable to multiple-master time series. In the work presented here I use a new statistical cost flow algorithm applicable to single- or multiple-master time series (A. Hooper, A statistical cost approach to unwrapping the phase of SAR interferogram time series, manuscript in preparation, 2008).

2.2.1. Small Baseline Interferograms

[9] In order to maximize the correlation of the interferograms formed, small baseline methods seek to minimize the *perpendicular, temporal* and *Doppler baselines*, that is, the component of the physical separation between the two satellite acquisition positions perpendicular to the line-of-sight, the separation in time, and the difference between the Doppler centroids of acquisition pairs. I select image pairs whose estimated correlation is above a threshold value, which depends on the expected rate of decorrelation for the given terrain and the data availability for the specific application, while ensuring that the resultant network of image-pairs contains no isolated clusters (Figure 1). A minimum of five images are required, although in practice more are usually necessary to satisfy the minimum correlation requirements. The interferograms are formed by recombination of the resampled SLC images from the PS processing, first filtering in azimuth to exclude non-overlapping Doppler spectrum, and in range to reduce the effects of geometric decorrelation. Geometric phase is simulated from orbital ephemerides and a digital elevation model, and subtracted.

2.2.2. SDFP Pixel Selection

[10] SDFP pixels are defined by their phase characteristics, however, computational burden can be reduced by selecting an initial subset of pixels that is expected to include almost all SDFP pixels, through analysis of amplitudes. For Gaussian scatterer pixels an indication of the phase stability is given by the amplitude difference dispersion, defined here as $D_{\Delta\mathcal{A}} \equiv \sigma_{\Delta\mathcal{A}}/\mu_{\mathcal{A}}$, where $\sigma_{\Delta\mathcal{A}}$ is the standard deviation of the difference in amplitude between master and slave, and $\mu_{\mathcal{A}}$ is the mean amplitude. This is similar to the amplitude dispersion index ($D_{\mathcal{A}}$) derived by *Ferretti et al.* [2001] for point scatterers, however, $D_{\Delta\mathcal{A}}$ is a better estimate of phase stability in the case where spectral filtering has been applied (see Auxiliary Material[1] for derivation and discussion.) For the data presented in this manuscript a threshold value of $\widehat{D}_{\Delta\mathcal{A}} \leq 0.6$ was used to reduce the data set size.

[11] SDFP pixels are identified among the candidate pixels in the same way that PS pixels are, using the algorithm of *Hooper et al.* [2007], which differs from "standard" PS identification algorithms. The spatially-correlated contribution to the interferometric phase of a pixel is estimated by bandpass filtering of surrounding pixels. This is assumed to include the phase due to ground displacement, temporal change in atmospheric delay, orbital inaccuracies and spatially-correlated height error. A spatially-uncorrelated look angle error term, which includes contributions from both spatially-uncorrelated height error and deviation of the pixel's phase center from its physical center, is then estimated through its correlation with perpendicular baseline. Subtraction of these two estimates leaves an estimate of the decorrelation noise for a pixel, which is then characterized in terms of a measure similar to coherence magnitude,

$$\gamma_x = \frac{1}{N}\left|\sum_{i=1}^{N} \exp\{\sqrt{-1}\left(\psi_{x,i} - \widetilde{\psi}_{x,i} - \Delta\widehat{\phi}^{u}_{\theta,x,i}\right)\}\right|, \qquad (1)$$

where $\psi_{x,i}$ is the wrapped phase of pixel x in the ith interferogram, $\widetilde{\psi}_{x,i}$ is the estimate of the spatially-correlated terms, $\widehat{\phi}^{u}_{\theta,x,i}$ is the estimate of the spatially-uncorrelated look angle error term and N is the number of interferograms. Statistical analysis of the distribution of γ_x and $D_{\Delta\mathcal{A}}$ values yields a threshold function, $\gamma_x^{thresh}(D_{\Delta\mathcal{A}})$, for pixel selection.

[1] Auxiliary materials are available in the HTML. doi:10.1029/2008GL034654.

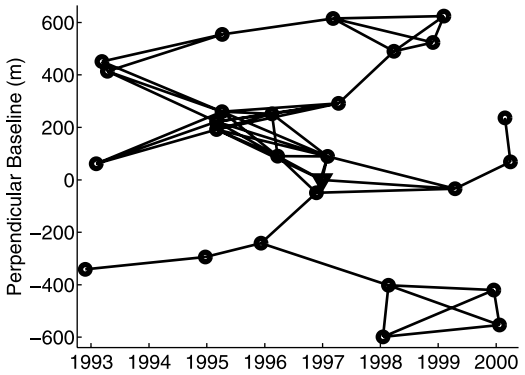

Figure 1. Baseline plot. The triangle represents the master image used in the PS processing, circles represent the other images, and lines represent the SB interferograms formed. Doppler separation for the image-pairs is not shown, but in most cases is less than 100 Hz, with a maximum value of 720 Hz.

This threshold function depends on a user-specified value for the required certainty that the phase of a selected pixel is not random. Note that although the same algorithm is used to select both PS and SDFP pixels, different sets of pixels are chosen because the algorithm is applied to different sets of interferograms: single master with no spectral filtering vs. multiple master with spectral filtering.

2.3. Combined Data Set Processing

[12] Because the phase is measured modulo 2π radians, integer phase-cycle ambiguities must be estimated in order to derive the deformation field, a process known as *phase unwrapping*. The problem of phase unwrapping is inherently non-unique, but increasing the spatial sampling reduces the chances of spatial aliasing and thereby increases the chances of success. The selected PS and SDFP pixels are therefore combined before this step to maximize the reliability of the unwrapped phase.

[13] In order to combine the data sets the equivalent SB interferogram phase is calculated for the PS pixels by recombination of single-master interferogram phase. Note that this equivalent SB phase is different to that extracted from the small baseline interferograms directly, because no spectral filtering has been applied. A revised estimate of γ_x (equation (1)) is calculated for PS pixels from the resulting SB interferogram phase. This is usually lower than the value calculated from the single-master interferogram phase, where the master contribution to the decorrelation term is present in every interferogram and does not therefore contribute to the variation, and is directly comparable to the estimate of γ_x for SDFP pixels. The SB interferogram phase from both PS and SDFP pixels is then combined. When a pixel occurs in both data sets, a weighted mean value for the phase is calculated by summing the complex signal from both data sets, with the amplitude of each fixed to an estimate of the signal-to-noise ratio (SNR) for the pixel in that data set. The SNR is estimated as [*Just and Bamler*, 1994]

$$\widehat{SNR} = \frac{1}{\gamma_x^{-1} - 1}. \quad (2)$$

[14] The phase of the combined data set is corrected using the estimate of spatially-uncorrelated look angle error calculated in the selection steps. The method of Hooper (manuscript in preparation, 2008) is then applied to unwrap the resulting phase of each combined SB interferogram. Phase unwrapping of SB interferograms, which cover short time intervals, as opposed to single-master interferograms has the added advantage of reducing spatial-aliasing in the case of high deformation rates.

[15] The unwrapped phase of the SB interferograms must be inverted to derive a time series of phase change for each pixel. *Berardino et al.* [2002] perform the inversion using singular value decomposition, imposing an extra minimum-norm constraint. As I ensure that there are no isolated clusters of interferograms in my analysis, this extra constraint is not required and I invert the unwrapped phase in a least-squares fashion, similar to *Schmidt and Bürgmann* [2003]. The model phase retrieved is then the phase of each pixel relative to an arbitrary reference pixel and master image. To check that the phase for all SB interferograms contributing to each final single-master interferogram is consistent, I calculate the residual phase between the SB interferograms and the phase predicted by the model single-master interferograms. Residuals of up to 2π are expected for individual pixels, due to local phase-unwrapping errors, but any spatially-correlated residuals imply systematic phase-unwrapping errors. If this is the case, problem interferograms can be identified and their phase unwrapped more carefully, or they can be dropped from the inversion if the redundancy of the SB interferograms allows.

3. Application to Eyjafjallajökull

[16] I applied the combined MT-InSAR method to 27 images acquired by ERS-1 and ERS-2 satellites over Eyjafjallajökull volcano between May 1993 and September 2000 (Figure 1).

[17] The same certainty threshold of 99% for pixel selection was used for both methods. Using the PS method 177,000 PS pixels were identified, as opposed to 659,000 with the SB method, implying that there are more ground resolution elements containing a distribution of semi-stable scatterers than those dominated by a single scatterer. This is apparently true even in areas where coherent pixels are sparse, for example, the ice caps where a few rocks (nunataks) project through, and the farmed areas along the coast (Figure 2, left and middle). Of the selected pixels, 133,000 were selected by both methods. Dropping the certainty threshold for PS pixel selection to 90% led to a greater proportion of the pixels being selected by the PS method only, indicating that PS pixels are not merely a subset of SDFP pixels. Figure 2 (right) shows γ_x for both methods, for pixels included as a candidate by both methods and selected by at least one method. For most pixels, γ_x is higher using the SB method, implying that these pixels are closer to the Gaussian scatterer model and spectral filtering decreases noise. The remainder of the pixels are presumably closer to the point scatterering model and spectral filtering adds noise.

[18] Results from the combined method are shown in Figure 3. There were two intrusive episodes, the first of which occurred in 1994 and the second of which began in

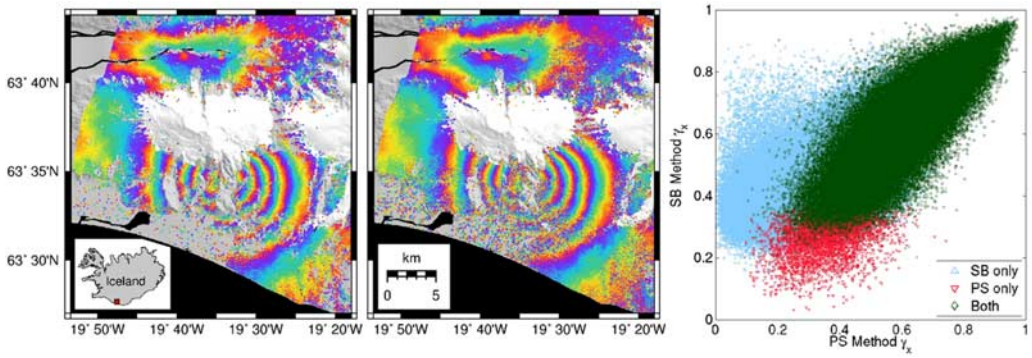

Figure 2. Comparison of pixels on and around Eyjafjallajökull volcano selected by both methods. (left) Pixels selected by the PS method of *Hooper et al.* [2007] and (middle) pixels selected by the SB method described in this paper. The pixels are plotted on topography in shaded relief, with white representing the approximate area of permanent ice cover. The location of the area analyzed is shown left inset. 27 images were used in the analysis although only one interferogram is shown here, which covers 27 June 1997 to 10 October 1999. Each color fringe represents 2.8 cm of displacement in the line-of-sight and in both cases the phase of the selected pixels has been filtered using an adaptive phase filter [*Goldstein and Werner*, 1998]. (right) Comparison of γ_x, which is an estimate of coherence magnitude, for all pixels selected by either method that were included as candidate pixels by both methods.

1999 and ended in early 2000 [*Pedersen and Sigmundsson*, 2006]. The deformation caused by the two episodes is clearly centered at different locations, which was also the conclusion of *Pedersen and Sigmundsson* [2006] from conventional InSAR analysis. The overall deformation pattern for each episode is more spatially even than deduced from conventional InSAR, however, due to the removal of digital elevation model and atmospheric artifacts, and more accurate phase unwrapping in the multi-temporal analysis. The four time steps covering the second intrusive episode show a clear progression of the deformation field, which correlates partly with the migration of the seismicity (Figure 3). The minimum strain detected in this case is $\sim 10^{-5}$. In general, the limiting factor on deformation detection is the ability to distinguish it from atmospheric phase delay variation and orbit error, which depends on the

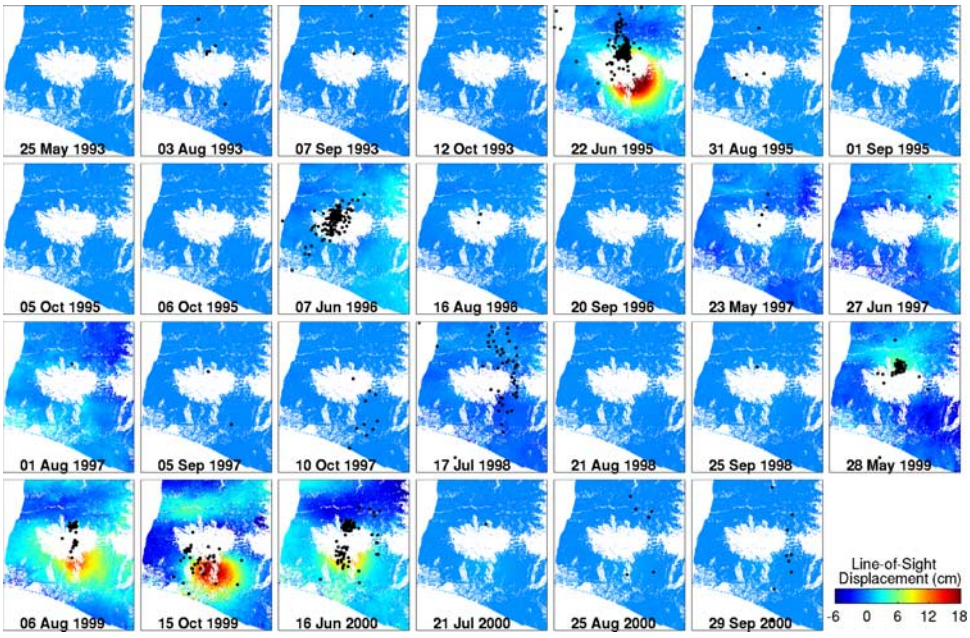

Figure 3. Time series of line-of-sight displacement for Eyjafjallajökull volcano from combined MT-InSAR method. Each image represents the incremental displacement towards the satellite since the time of the previous image, relative to pixels in the northwest corner. Phase due to atmospheric delay and orbit errors has been estimated and removed by spatio-temporal filtering following *Hooper et al.* [2007], except for the 1999 images where the temporal sampling rate is not high enough with respect to the change in deformation rate to separate these terms from displacement. Black dots represent catalogue epicenter locations from the SIL database of the Icelandic Meteorological Office, for $M_0 \geq 0.5$ earthquakes occurring in the corresponding time interval. Only epicenters west of 19°26W are shown to exclude most earthquakes associated with Katla volcano, which abuts Eyafjallajökull to the east.

magnitude of these non-deformation terms and the degree of temporal correlation of the deformation.

4. Conclusions

[19] The combined MT-InSAR algorithm presented here combines the phase of selected pixels from spectrally-filtered interferograms (small baseline method) with the phase of selected pixels from interferograms with no spectral filtering (persistent scatterer method). This results in more pixels being selected than are selected by either method alone, in other words, the spatial sampling is improved. For pixels selected by both approaches, the SNR is also increased. The algorithm was applied to Eyjafjallajökull volcano, for an interval in which two intrusion episodes occurred, and a time series for the displacement field was retrieved that is consistent with the seismicity.

[20] **Acknowledgments.** I thank Ramon Hanssen and the anonymous reviewers for their comments. ERS data were provided by the European Space Agency. Focused SAR images were produced using the ROI_PAC software package developed by the Jet Propulsion Laboratory. Some interferometric processing was performed with the Doris software package developed by Delft University of Technology. This research was supported by the European Commission, 6th Framework Project 'VOLUME', contract 08471.

References

Berardino, P., G. Fornaro, R. Lanari, and E. Sansosti (2002), A new algorithm for surface deformation monitoring based on small baseline differential SAR interferograms, *IEEE Trans. Geosci. Remote Sens.*, *40*(11), 2375–2383.

Ferretti, A., C. Prati, and F. Rocca (2001), Permanent scatterers in SAR interferometry, *IEEE Trans. Geosci. Remote Sens.*, *39*(1), 8–20.

Gatelli, F., A. M. Guamieri, F. Parizzi, P. Pasquali, C. Prati, and F. Rocca (1994), The wavenumber shift in SAR interferometry, *IEEE Trans. Geosci. Remote Sens.*, *32*(4), 855–865.

Goldstein, R. M., and C. L. Werner (1998), Radar interferogram filtering for geophysical applications, *Geophys. Res. Lett.*, *25*(21), 4035–4038.

Hooper, A., and H. Zebker (2007), Phase unwrapping in three dimensions with application to InSAR time series, *J. Opt. Soc. Am. A Opt. Image Sci.*, *24*, 2737–2747.

Hooper, A., H. Zebker, P. Segall, and B. Kampes (2004), A new method for measuring deformation on volcanoes and other natural terrains using InSAR persistent scatterers, *Geophys. Res. Lett.*, *31*, L23611, doi:10.1029/2004GL021737.

Hooper, A., P. Segall, and H. Zebker (2007), Persistent scatterer interferometric synthetic aperture radar for crustal deformation analysis, with application to Volcán Alcedo, Galápagos, *J. Geophys. Res.*, *112*, B07407, doi:10.1029/2006JB004763.

Just, D., and R. Bamler (1994), Phase statistics of interferograms with applications to synthetic-aperture radar, *Appl. Opt.*, *33*(20), 4361–4368.

Kampes, B. M. (2005), Displacement parameter estimation using permanent scatterer interferometry, Ph.D. thesis, Delft Univ. of Technol., Delft, Netherlands.

Lanari, R., O. Mora, M. Manunta, J. J. Mallorqui, P. Berardino, and E. Sansosti (2004), A small-baseline approach for investigating deformations on full-resolution differential SAR interferograms, *IEEE Trans. Geosci. Remote Sens.*, *42*(7), 1377–1386.

Pedersen, R., and F. Sigmundsson (2006), Temporal development of the 1999 intrusive episode in the Eyjafjallajökull volcano, Iceland, derived from InSAR images, *Bull. Volcanol.*, *68*, 377–393.

Pepe, A., and R. Lanari (2006), On the extension of the minimum cost flow algorithm for phase unwrapping of multitemporal differential SAR interferograms, *IEEE Trans. Geosci. Remote Sens.*, *44*(9), 2374–2383.

Schmidt, D. A., and R. Bürgmann (2003), Time-dependent land uplift and subsidence in the Santa Clara valley, California, from a large interferometric synthetic aperture radar data set, *J. Geophys. Res.*, *108*(B9), 2416, doi:10.1029/2002JB002267.

van der Kooij, M., W. Hughes, S. Sato, and V. Poncos (2006), Coherent target monitoring at high spatial density: Examples of validation results, Eur. Space Agency Spec. Publ., *SP-610*.

Zebker, H. A., and J. Villasenor (1992), Decorrelation in interferometric radar echoes, *IEEE Trans. Geosci. Remote Sens.*, *30*(5), 950–959.

A. Hooper, Department of Earth Observation and Space Systems, Delft University of Technology, Kluyverweg 1, NL-2629 HS Delft, Netherlands. (a.j.hooper@tudelft.nl)

Auxiliary Material for 'A Multi-Temporal InSAR Method Incorporating Both Persistent Scatterer and Small Baseline Approaches'

Andrew Hooper

S1. Amplitude Difference Dispersion

For Gaussian scatterer pixels the joint probability density function (PDF) for interferometric phase, ψ, is given by [*Just and Bamler*, 1994]

$$PDF(\psi) = \frac{1-|\rho|^2}{2\pi} \frac{1}{1-|\rho|^2 cos^2(\psi-\psi_0)} \quad (1)$$

where ρ is the complex correlation coefficient, or *coherence*, and ψ_0 is the expected interferometric phase for zero decorrelation. For high coherence ($\rho > 0.8$) this distribution approaches a Gaussian distribution with standard deviation σ_ψ, where σ_ψ is an indicator of the phase stability of the pixel. From complex plane geometry, for a single pixel in a single interferogram, the interferometric phase due to decorrelation, $\psi - \psi_0 \approx n_\perp / \mathcal{A}_m$, where $n_\perp$ is the component of the complex decorrelation noise, n, perpendicular to the master complex vector and $\mathcal{A}_m$ is the master amplitude. For high coherence, n approaches a circular Gaussian distribution, and $\sigma_\psi \approx \sigma_{n\perp}/\mu_\mathcal{A}$, where $\sigma_{n\perp}$ is the standard deviation of $n_\perp$ and $\mu_\mathcal{A}$ is the mean amplitude. But for circular Gaussian n, $\sigma_{n\perp} = \sigma_{n\parallel} \approx \sigma_{\Delta\mathcal{A}}$ where $\sigma_{n\parallel}$ is the standard deviation of the parallel component of n and $\sigma_{\Delta\mathcal{A}}$ is the standard deviation of the difference in amplitude between master and slave. Therefore $\sigma_\psi \approx \sigma_{\Delta\mathcal{A}}/\mu_\mathcal{A}$. This quantity which I define as the amplitude difference dispersion, $D_{\Delta\mathcal{A}}$, is an indicator of SDFP phase stability, for high coherence at least. Although derived from the phase statistics of Gaussian scatterers, $D_{\Delta\mathcal{A}}$ is similar in form to the amplitude dispersion index ($D_\mathcal{A}$) derived by *Ferretti et al.* [2001] from the phase statistics of point scatterers. In the case of interferograms formed from images that are not spectrally-filtered $D_{\Delta\mathcal{A}} \approx \sqrt{2} D_\mathcal{A}$, with $\sigma_\psi \approx D_\mathcal{A}$ applicable in the single master case, when only variation in slave phase contributes to variation in interferometric phase and $\sigma_\psi \approx D_{\Delta\mathcal{A}}$ applicable in the multiple master case, when variation in the master phase also contributes. For interferograms formed from spectrally-filtered images, however, this approximate relationship between $D_\mathcal{A}$ and $D_{\Delta\mathcal{A}}$ no longer holds as $D_\mathcal{A}$ includes variation in the entire bandwidth of each image whereas $D_{\Delta\mathcal{A}}$ includes only the variation in the retained parts of the spectra for each interferogram. $D_{\Delta\mathcal{A}}$ is a better estimate of σ_ψ than $\sqrt{2} D_\mathcal{A}$ in this case because it is also only the retained parts of the spectra that contribute to σ_ψ.

The results of simulated interference between Gaussian scatterers with varying degrees of decorrelation are shown in auxiliary Fig. S1.

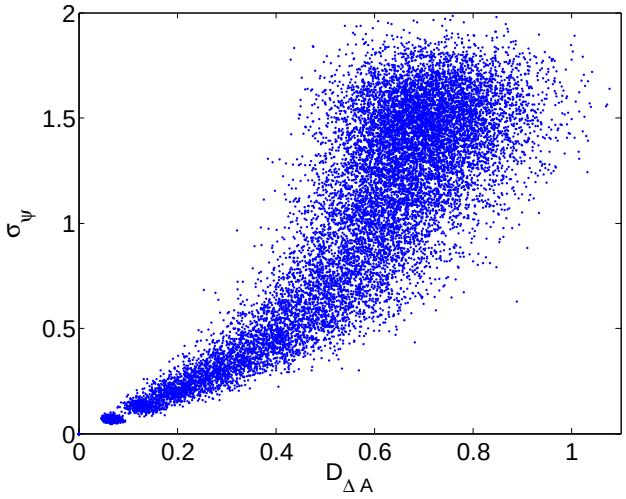

Figure S1. *Numerical simulation results for Gaussian scatterer resolution elements. Each resolution element consists of 100 scatterers with real and imaginary parts drawn from a random normal distribution with a standard deviation of one. Decorrelation is simulated by varying the real and imaginary parts for each of the scatterers within the cell, by an amount drawn from a random normal distribution, the standard deviation of which is incremented from zero to two. For each increment 34 independent values for the resolution element are simulated, from which 68 interfered values are calculated, and this is repeated 5000 times.*

References

Ferretti, A., C. Prati, and F. Rocca, Permanent scatterers in SAR interferometry, IEEE Trans. Geosci. and Remote Sens., 39(1), 8 – 20, 2001.

Just, D., and R. Bamler, Phase statistics of interferograms with applications to synthetic-aperture radar, Applied Optics, 33(20), 4361–4368, 1994.

A. Hooper, Delft University of Technology, Kluyverweg 1, 2629 HS Delft, The Netherlands (a.j.hooper@tudelft.nl)